

Optical Imaging in Biology and Medicine
Master in Photonics & Europhotonics Master Program

Adaptive Optics for Microscopy

Carles Otero Molins

Johannes Rebling

November 30, 2013

Abstract

To achieve optimal, diffraction limited images with the best possible resolution has always been a challenging topic and an important goal in science in general and in biophotonics in particular. Although many new techniques to acquire superresolution images were developed in the last decade, unwanted aberrations often still compromise the resolution and brightness of the images taken with these techniques. Adaptive Optics (AO), a technique that originated in astronomy, is a possible solution to compensate for aberrations in biomedical imaging.

This report presents a review of the numerous applications of AO applied to modern microscopy methods. We review the basic principles of AO, describe how the aberration information is obtained (via direct and indirect sensing) and how AO is applied in the main microscopy techniques (widefield and point scanning techniques). We show that AO methods have been applied in almost all modern microscopy techniques. However, the increase in resolution and signal quality depends strongly on both the AO and the microscopy technique and great care has to be taken when trying to implement the optimal AO technique.

Contents

| | | |
|-------------------|---|-----------|
| 1 | Introduction | 1 |
| 2 | Aberration Measurement and Correction | 1 |
| 2.1 | Direct Wavefront Sensing | 2 |
| 2.2 | Indirect Wavefront Sensing | 4 |
| 2.2.1 | Genetic and Random Optimization | 4 |
| 2.2.2 | Model Based Optimization | 7 |
| 2.3 | Aberration Correction | 8 |
| 3 | Adaptive Optics Methods applied in Microscopy | 8 |
| 3.1 | Widefield Microscopy | 9 |
| 3.1.1 | Direct Wavefront Sensing in a Transmission Microscope | 9 |
| 3.1.2 | Indirect Wavefront Sensing in a Transmission Microscope | 10 |
| 3.1.3 | Structured Illumination Microscopy | 12 |
| 3.2 | Point Scanning Microscopes | 13 |
| 3.2.1 | Confocal Microscopes | 14 |
| 3.2.2 | Two-Photon Fluorescence Microscopy | 15 |
| 3.2.3 | Multiphoton Scanning Microscopy using Indirect sensing. | 15 |
| 3.2.4 | TPFM Direct | 17 |
| 4 | Conclusion & Future Prospects | 21 |
| References | | 22 |

1 Introduction

It is well known that optical aberrations degrade the resolution and brightness of images. This results in a reduction of both lateral and axial resolution and a decrease in signal intensity. In general aberrations can be defined as the wavefront distortions with respect to an ideal sphere. These distortions can be caused by imperfections and inhomogeneities in any part of the optical system. In microscopy, aberrations may arise from the microscope itself or the specimen under study [1]. Aberrations always limit the final image quality and can vary from one specimen to another. In this case they can not be corrected by a optimized optical design which makes dynamic correction necessary.

It is of little surprise that scientists have been trying to overcome this problem for many years, an effort that resulted in what nowadays is called Adaptive Optics (AO). The first proposal of the use of AO technology was suggested in the year 1953 in the context of astronomical optics for the compensation of the aberrating effects of the atmosphere [2].

The main idea of AO is the modulation of an incoming wavefront in such a way that we can record an image without aberrations. It is based upon the principle of phase conjugation: the correction element introduces an equal but opposite phase aberration to that present in the optical system. In order to do that, we need to be able to measure these distortions reliably. The most direct way is to use a wavefront sensor, such as the Shack-Hartmann [3, 4] or Curvature Sensors [5]. Also, interferometric techniques have been used to measure aberrations [6]. Furthermore, there are indirect or sensorless methods in which aberrations are determined using an optimization algorithm and do not employ a direct wavefront sensing [7]. A control system then processes the aberration information and uses it to control and adaptive correction element. The adaptive element is needed to modulate and correct the incoming wavefronts before the light reaches the imaging detector. This task is usually performed by a deformable mirror or a liquid crystal spatial light modulator (LC-SLM).

Although Adaptive Optics systems have been successfully introduced in applications such as astronomy, laser beam shaping, optical communications, data storage and ophthalmology [8], it is not trivially applied to microscopy. One particularly difficult problem in AO microscopy is how the aberration information is obtained in each of the different microscopy techniques, since direct sensing can usually not be easily implemented as it is the case in astronomy.

Optical microscope techniques can be divided in two main groups: the widefield techniques and the point scanning techniques. Examples of the first group are the conventional transmission microscopy, the structured illumination microscopy and the fluorescence microscopy. Some point scanning techniques are the confocal microscopy, Stimulated Emission Depletion (STED) or the non-linear microscopy such as Two-Photon Excitation Fluorescence (TPEF), Second Harmonic Generation (SHG) microscopy, Third Harmonic Generation (THG) microscopy and Coherent anti-Stokes Raman (CARS).

In order to explain how adaptive optics and microscopy are linked together, we will start explaining the basis of adaptive optics. This includes a brief review of the concept of aberrations and how they are most commonly characterized. After that, we will explain in more detail the main methods for wavefront sensing, the main aberration corrector devices and some control strategies. Furthermore, we will show some applications of the AO in different widefield and point scanning microscopy techniques. The last part will be a short explanation of future prospects and conclusions.

2 Aberration Measurement and Correction

In practice, no optical system can be totally free from aberrations. That means that all the rays originating from the same object point and going through an optical system will not converge into the same point at the image plane. In other words, the wavefront is distorted with respect to an ideal one when passing through a real system. Thus, we can define the wavefront aberration function as the optical path difference between the aberrated (real) wavefront and the reference (perfect) wavefront. These aberrations can be introduced both upon reflection from a non-planar surface and by passing through an inhomogeneous media as shown in Fig. 1.

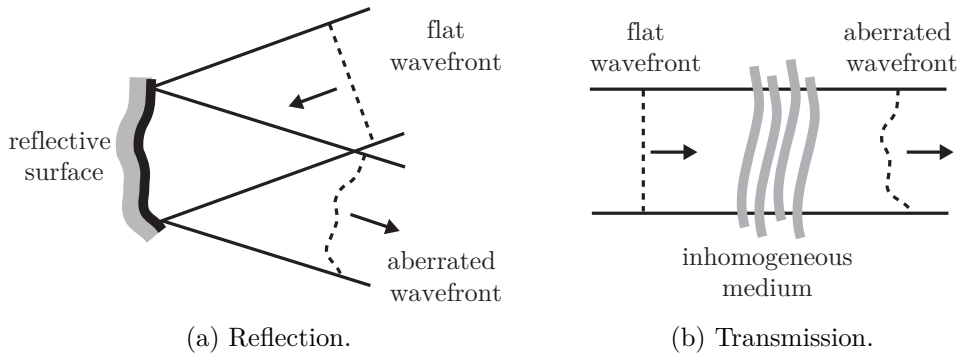


Figure 1: Wavefront aberrations due to (a) reflection from a non planar surface and (b) caused by propagation through a non-uniform refractive index distribution [1].

In biological microscopy, the two potential sources of aberrations are the optics and the specimen under study. Regarding the optics, one important parameter is the Numerical Aperture (NA) since aberrations become more significant for those microscopes employing higher NA objectives. Aberrations can also be produced by the difference of refractive index between the microscope coverslip and the specimen mounting medium. Regarding the specimen, aberrations are caused by the variations in refractive index due to the three-dimensional nature of cells and tissue structures. These sample induced aberrations generally become dominant when the image focus lies deep within the sample, since light has to pass a large distance through an inhomogeneous medium [1].

There are different ways to characterize the aberrations mathematically. In systems with circular symmetry (circular apertures) it is very common to use the Zernike polynomials because they form a complete, orthogonal set of functions defined over a unit circle [9]:

$$W(\rho, \phi) = \sum_n \sum_{m=-n}^{m=n} c_n^m Z_n^m(\rho, \phi), \quad (2.1)$$

where $W(\rho, \phi)$ is the wavefront aberration function in polar coordinates at the exit pupil, c_n^m are the Zernike coefficients and $Z_n^m(\rho, \phi)$ are the Zernike modes (or polynomials). As we can see in the equation, the wavefront aberration function is a linear combination of polynomials. Therefore, the more polynomials (i.e. modes, $Z_n^m(\rho, \phi)$) we can measure, the better characterization of the $W(\rho, \phi)$ function we have. Representing aberrations in this way can simplify the design, control and characterization of the Adaptive Optics system.

Although it is known where the aberrations come from, it is not always easy to measure them and implement the measure inside the optical system. There are different classifications of wavefront sensing in the bibliography [10]. Here we will use the one employed by *Martin J. Booth* [1] and we will explain the most common methods of wavefront sensing applied to microscopy.

2.1 Direct Wavefront Sensing

Direct Wavefront Sensing is based on a direct measure of the phase gradient or the wavefront slope, it is considered as an aperture-plane sensing. Within this group there are several techniques such as interferometric, although in general the most used is the Shack-Hartmann.

The Shack-Hartmann technique is based on a two-dimensional array of a few lenslets, a matrix of micro-lenses, all with the same diameter and the same focal length. The aberrated wavefront is divided into smaller sub-wavefronts and then imaged by the separated micro-lenses onto a detector. The micro-lens matrix forms multiple focus spots in the focal plane and the recording device placed at the focal plane of the matrix records multiple spots, as shown in Fig. 2. The recording device is usually a CCD camera and typical micro-lens diameters range from about 100 to 600 mm with typical focal lengths ranging from a few millimeters to about 30 mm [11]. By measuring the displacements ($\Delta x, \Delta y$) of each focal spot created by the separate microlenses (Fig. 2) allows to reconstruct the wavefront slopes and

finally to reconstruct the wavefront aberration function.

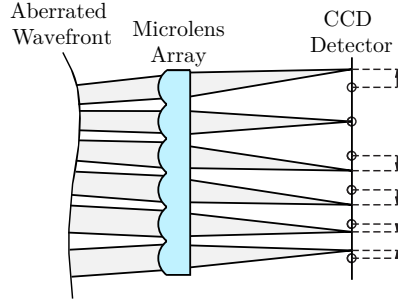


Figure 2: Two-dimensional section of Shack-Hartmann matrix of microlens. An incoming wavefront is divided in multiple, smaller sub-wavefronts and imaged onto a CCD detector by a microlens array. This generates separate focal spots for each microlens. If the wavefront is not aberrated, each spot will be placed along the central axis of each microlens. If it is aberrated, it will be displaced with respect to this axis and a wavefront reconstruction can be performed based on the magnitude and direction of this displacement. Image after [12].

While the basic idea of this sensing techniques is simple, we must note that a well defined wavefront in the pupil of the system is required which can only be produced by a point-like emitter. When studying three-dimensional, biological specimens, a single point like emitter is usually not encountered which leads to a number of problems. The first one is the superposition of wavefronts which depends on the coherence of the emitted light. Coherent light will cause interference in the pupil, thus causing ambiguous sensor readings rendering the measurement useless for aberration correction.

If the specimen behaves as a point-like scatterer, it will emit incoherent light and the sensor is able to measure the aberrations produced in the emission path. If a reflection and not a transmission setup is used, the aberrations in the emission path should be the same as in the illumination path. However, if the specimen acts like a planar mirror in the focal region, the sensor will just be able to measure twice the even components of the aberrations produced in the illumination path (or emission path). This is caused by the spatial inversion caused by any mirror, as shown in Fig. 3). Hence we lose information part of the information about aberrations. Thus, implementing a direct sensing in this cases it is not a good option and indirect sensing schemes should be preferred.

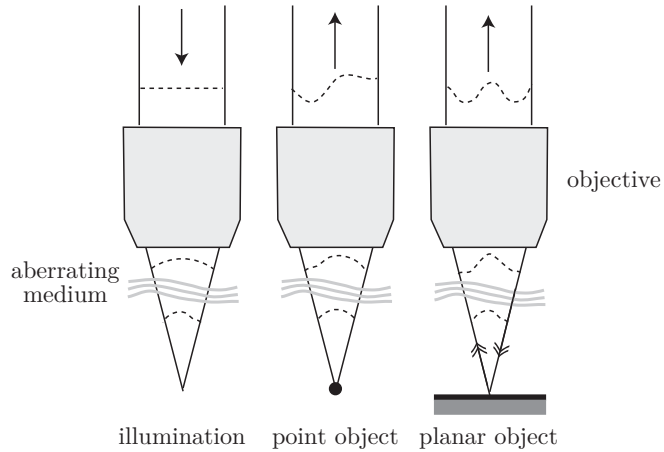


Figure 3: Representation of the two effects due to the specimen structure on wavefront measurements. The left figure shows how the wavefront is aberrated in the illumination path. In the center it is shown a point-like scatterer. Only the emission path is measured. In the right figure it is shown a planar reflector. The illumination wavefront is spatially inverted on reflection before acquiring further aberration in the detection path. Image after [1].

Another problem that can arise is due to three-dimensional nature of the specimen. The sensor might detect more signal intensity from the light scattered from out-of-focus areas rather than from the focal

region. In order to overcome this problem, a spatial filter between objective and sensor can be used, much like the pinhole used in confocal microscopy. It is also possible to use coherence gating to exclude out-of-focus light instead of the spatial filter, although it is a more complex method [13].

2.2 Indirect Wavefront Sensing

While direct wavefront sensing techniques are widely applied in astronomy, they are less common in microscopy techniques. This for several reasons. It is not as easy to create a “guide-star” like point source in a biological specimen. If there are no features in the specimen that occur naturally and which resemble a point source, one has to be implemented them manually which might alter the function of the specimen or might even be toxic to the sample. Modern microscopes are also highly complex and optimized, which makes it difficult to insert a relatively large wavefront sensor. For samples with weak signal strength, it is also desirable to collect as many photons as possible for the imaging process. Splitting the beam and using a part of the light emitted from the sample for direct wavefront sensing might hence decrease the signal strength or increase the recording time too much.

Indirect techniques do not measure the wavefront directly but instead optimize some merit function (also called quality metric) that depends on the optical system. Indirect methods are used more often in industrial and medical applications. They usually require very little additional hardware. Once the technique is optimized for a specific problem, indirect schemes are easier to implement in practice and are more prone to errors due to the lack of additional hardware (a single deformable mirror might be sufficient to implement adaptive optics in an existing microscope).

For these techniques, the optimization of an image quality metric is mainly a mathematical rather than a technical problem. The aberration correction is performed through an iterative optimization of an image quality metric. The metric is usually based on spatial frequencies [14] or image intensity [15] and gives a mathematical measurement of how “good” the recorded image is. In many practical systems aberrations can be accurately represented by a small number of modes of an orthogonal basis, such as Zernike polynomials. The optimization is then performed by adapting the polynomial coefficients applied to the deformable mirror either stochastically or by using an appropriate mathematical model.

2.2.1 Genetic and Random Optimization

For the stochastic methods there are several algorithms, one of the most popular being genetic algorithms [16]. These algorithms try to find an optimal solution by simulating an evolution process. The implementation of a genetic algorithm in AO begins with a population of typically random sets of Zernike polynomials, called initial population. The separate members of the population are called chromosome (also called genotype). After creating this initial population, each chromosome is evaluated and assigned a fitness value using the image quality metric. Then, a selection is applied to the population to create an intermediate population in a way that those chromosomes which represent a better solution are given more chances to “reproduce” than those chromosomes which are poorer solutions. Then recombination and mutation are applied to the intermediate population to create the next population. The process of going from the current population to the next population constitutes one generation. This process is repeated until a sufficiently good solution is found. These genetic algorithms do not require any preliminary information about the system but they are more time consuming than model-based approaches. Genetic algorithms are highly complex and a detailed description of the underlying principles and the separate steps is well beyond the scope of this report.

from [17]

this report is primarily concerned with the optimization of an image as a whole by selecting a particular point of interest and improving the brightness. The algorithms used are hill climbing (HC), genetic (GA), random search (RS), and adaptive random search (ARS). To the best of our knowledge, only the HC and GA have previously been used for this technique. These algorithms are compared in terms of the repeatability and reliability of the solutions, the final axial resolution of the system, and the time taken to complete an optimization.

The system used to test these algorithms was based on a reflection confocal microscope, shown schematically in Figure 1, although this method could also be applied to multiphoton microscopy.

The light reflected off the DMM was then focused using a 0.5-N.A. 20x (coverslip corrected) air microscope objective (Nikon) into a test sample. This lens has a working distance of 2.1 mm, making it a popular choice of objective lens by the life scientist and biologist for in-depth microscopy. Even at this relatively low N.A., aberrations are induced which when imaging at depth significantly degrade the image quality.

In the work presented here, the analogue signal was taken from the PMT and the intensity of a point was optimised and used as the fitness value or figure of merit.

The genetic algorithm (Man, 1999) works on an evolutionary basis, starting here with a population of 40 DMM shapes, which are assessed according to the fitness value and combined to produce an improved population of DMM shapes. The computer software allows the level of mutation and crossover to be set, which controls the generation of the new population.

For the four types of algorithms investigated here, two should (based upon statistical principles) determine the globally best solution to the DMM shape, whereas the HC and the ARS, although always reaching a maximum, may only reach a local maximum.

It can be seen that each algorithm significantly improves the peak intensity of the signal, and that as a consequence the FWHM of the system is reduced.

Although the solution for the hill climbing normally results in a higher FWHM, the advantage of using this algorithm is that it is much quicker than the other algorithms, always taking 48 seconds to complete compared to the maximum time taken by the genetic algorithm which was 12 minutes 30 seconds.

The exact choice of algorithm will largely depend on the application, and whether speed or ultimate resolution correction is paramount. The hill climbing proved to be the quickest routine and would probably be more suited to an initial investigation, or when the user was required to analyse a large quantity of samples, whereas if the aim was to gain the best possible image of one particular sample, the random search or genetic algorithm would be more appropriate. It is also possible to combine two different algorithms, for example starting with the RS to locate a region of DMM solution space and then speeding up the process by ending with the HC.

[18]:

The genetic algorithm is one of a group of stochastic optimization algorithms which is well-suited to finding a global minimum (or maximum) of some objective error function. In the context of adaptive-optical control, the genetic algorithm is well-suited to the task because of its ability to independently optimize many variables at once. In the case of a deformable mirror, each actuator voltage represents one independently adjustable variable. All stochastic algorithms work by assessing the quality of any proposed solution by defining an error function - normally a single number - whose value indicates how close any solution is to the target. In this way, deformable mirrors can be used together with evolutionary algorithms to optimize the laser beam shape. The genetic algorithm uses the concept of ‘survival of the fittest’ in evolution to locate the best solution to multidimensional problems. In the GA, first the control variables that are converted to binary codes are treated as genes. Second, selection from among the individuals and reproduction are performed in groups consisting of several individuals with different genes. Third, the individuals evolve because of mutations and crossovers. Mutation avoids converging to the local optima, and convergence to the global optimum is performed by crossover and selection. The basic GA’s are referred to as simple GA’s, and they repeat the following process from (b) to (d), so that a group becomes an optimum group as the number of generations increases:

- (a) Random generation of the initial group consisting of several individuals.
- (b) Calculation of the fitness value for each individual.
- (c) Selection and reproduction.
- (d) Crossover.
- (e) Mutation.

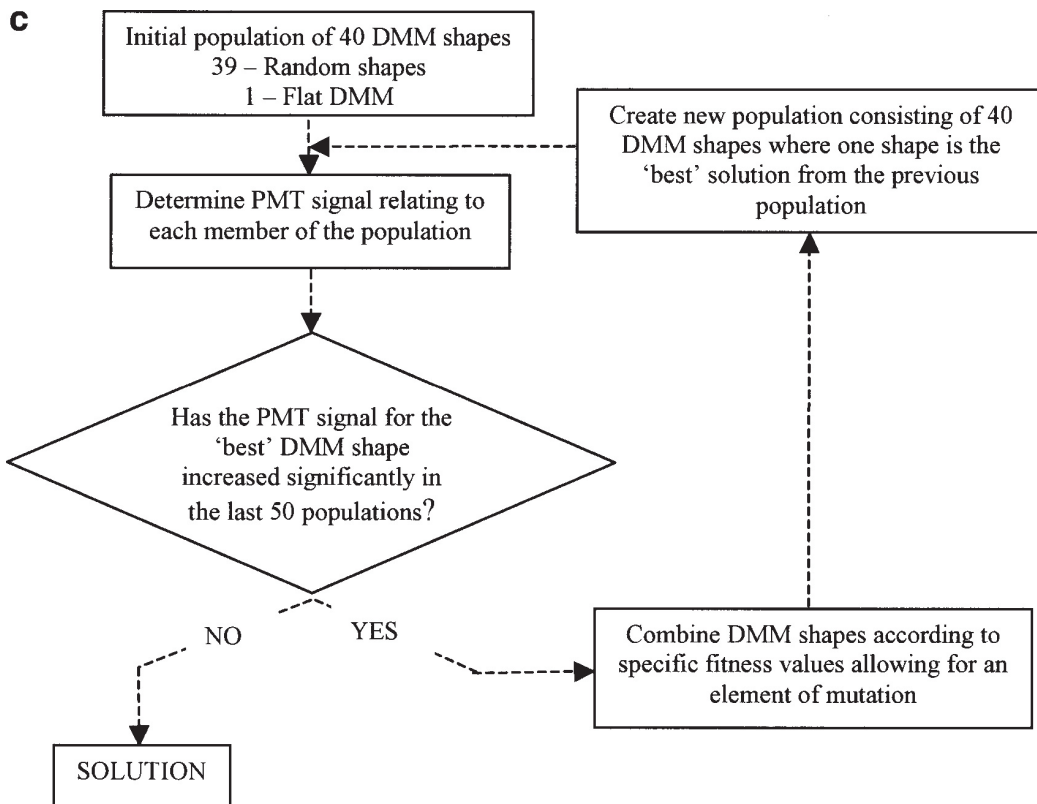


Figure 4: Genetica algortihm overview [17]

(f) Evaluation of the group.

The algorithm that we used in this study is shown in Fig. 5

It was found that 40 generations of 40 individuals with a crossover rate of 0.85 and a mutation rate of 0.2 would ensure a final solution close to the global maximum. The whole process would take about 15 minutes.

[19]:

The second algorithm uses an evolutionary algorithm,² which follows the Darwinian principle. Each membrane deformation is considered as an individual that is determined by a set of electrode voltages or by a set of Zernike polynomials.

A random population is designed and tested. The best individuals of this population are selected for reproduction. The reproduction is made by mixing the genetic code of the selection to create a progeny. During the mixing, a small part of the genetic codes undergoes a mutation, which is a random change of some codes. The obtained progeny is tested and compared to its parents. The best individuals from the comparison are selected to become the new parents. After several iterations, the best optimization is obtained.

There are many parameters to be specified for this algorithm. We chose to start with a random population of 500 individuals. The ten best are selected to create the progeny in the following manner: the three best individuals create 20 children and the ten best create 70 children, then these 90 children undergo a mutation and are compared to the ten parents. The 10 best individuals from these 100 individuals become the new parents. Only 1% of mutations are made on the first group of children and 10% are made on the second group.

For all four curves, the maximum is obtained after less than 8000 deformations, which has to be compared with the total number of possible deformations (4.53×10^{133}). The optimizations of the Zernike polynomials with both algorithms lead to an increase of the efficiency by a factor of at least 1.9. With the two algorithms working on the electrodes, the increase of efficiency goes up to a factor of 2.2. We notice also that the evolutionary algorithm applied to the electrodes improves the coupling faster than the others.

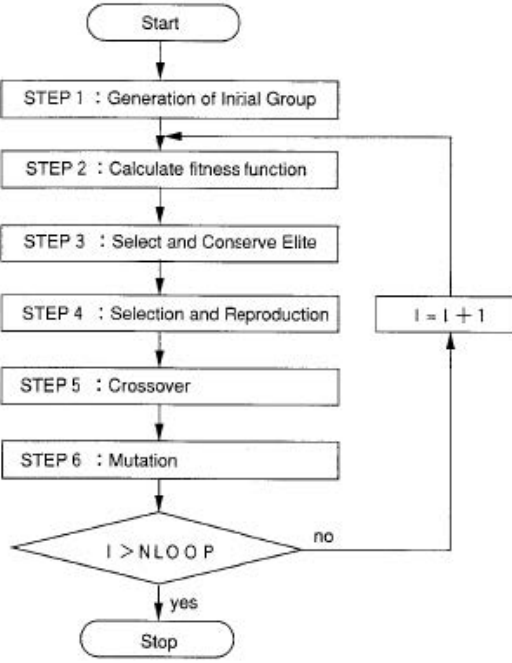


Figure 5: gnetic alog 2 [18]

[20]:

The optimization procedure is based on a genetic algorithm that maximizes the merit function that expresses the harmonic spectral intensity; 80 random actuator configurations are initially chosen and used as the starting point for the algorithm.

In conclusion, we have performed harmonic generation experiments using a deformable mirror in the beam path; the mirror, driven by a genetic algorithm, was exploited for optimization of the harmonic-conversion efficiency; we observed a marked increase in XUV emission after the optimization procedure was completed. From the analysis of the laser wave front, we infer that, in an optimal configuration, the DM reshapes the phase front

2.2.2 Model Based Optimization

Methods based on a mathematical model acquire a sequence of images, each with a different, predefined aberration applied. The correction aberration is estimated from the information in these images and this process is repeated until the image quality is considered acceptable. The number of measurements needed to obtain an acceptable image depends strongly upon the optimization algorithm and parameters used, the mathematical representation of the aberration, and the object structure. For the earliest and most generic algorithms the number of measurements per aberration mode increases quadratically or exponentially with N , the number of corrected aberration modes [21]. The so called direct maximization method (as described in Section 3.1.2) is significantly more efficient, requiring only $2N+1$ measurements for N mode. With this technique, Lukosz polynomials [22] are used to classify the aberrations. The effects of different modes can then be separated and the optimization of each mode becomes independent and hence more efficient.

An effective model-based adaptive optics scheme should also be independent of the imaged object and should permit the separation of aberration and object influences on the measurements. This separation is also possible through the appropriate choice of optimization metric and aberration representation [14]. The interested reader will find more information on the mathematical background in reference [23, 21, 22, 14].

2.3 Aberration Correction

The wavefront correctors are an essential part of an adaptive optics system. The goal is to apply a certain phase profile to the incident wavefront by changing either the physical length over which the wavefront propagates or the refractive index of the medium through which the wavefront passes. Wavefront correctors are built using either mirrors or liquid crystals. The former apply the phase change by adjusting their surface shape (i.e., change their physical length while keeping the refractive index constant) while the latter keep the physical length constant and rely on localized changes in refractive index. Mirror-based correctors are wavelength and polarization independent and can be reconfigured at rates of a few kilohertz [1]. They can have a continuous surface (i.e., discrete actuator, bimorph or membrane mirrors) or segmented surface (i.e. piston-only or piston/tilt mirrors) as shown in Fig. 6. Unlike continuous mirrors, the segmented mirrors have gaps between the segments that reduce the efficiency and quality of the correction, although they can achieve much better wavefront fitting.

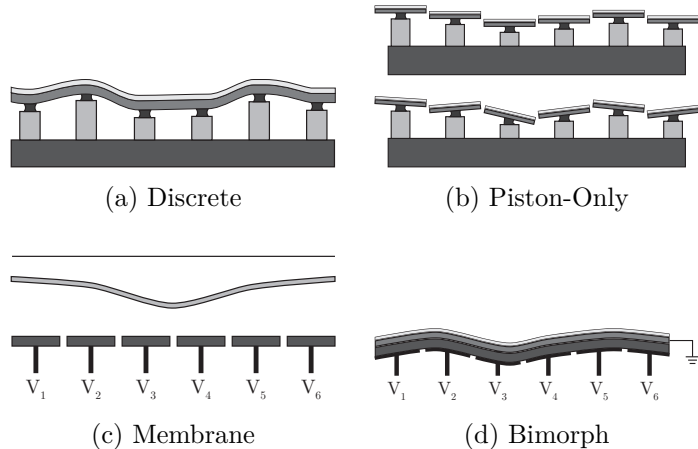


Figure 6: The four main mirror correctors. (a) Discrete actuator deformable mirrors consist of a continuous, reflective surface and an array of actuators, each capable of producing a local deformation in the surface. (b) Piston-only segmented correctors consist of an array of small planar mirrors whose axial motion (piston) is independently controlled. Piston/tip/tilt-segmented correctors add independent tip and tilt motion to the piston-only correctors. (c) Membrane mirrors and (d) Bimorph mirrors. Image after [11].

Liquid crystal-based modulators change the refractive index electronically or optically, are wavelength and polarization dependent and can reach velocities of just a few tens of hertz. The nematic liquid crystal is the most common for AO applications. In general, they are much cheaper than the mirror-based correctors, are capable of producing more complex phase patterns but they have lower light efficiency due to absorption.

In AO microscopes the first choice in most cases is the deformable mirror because of the higher efficiency. Furthermore, they are better suited for fluorescence techniques due to their polarization independent behavior. However, in particular cases, liquid-crystal modulators can be sufficient if aberration correction is only needed in the illumination path.

3 Adaptive Optics Methods applied in Microscopy

Adaptive optics techniques have found their way into almost all kinds of modern, high resolution microscopy techniques. These microscopes have been combined with direct wavefront sensing and sensorless AO, using deformable mirrors or spatial light modulators for aberration compensation (all of which has been described in Section 2). This includes standard widefield microscopes as well as highly sophisticated and specialized point scanning methods such as CARS and Stimulated Emission Depletion (STED) techniques. It has to be noted however, that some of these methods are themselves

only a few years old. Therefor, they are still being optimized and so are the AOM techniques. It is therefore an interesting field of research with new ideas being implemented every year.

AO was first used in confocal and two-photon fluorescence microscopy, both of which are commonly used in biomedical applications. These microscopes suffer from a significant drop in signal and resolution as the focus is moved deeper into the specimen, which is caused by aberrations [24].

AOM is also used for imaging of live specimens. Due to an increased excitation signal and improved light collection from the specimen, acquisition times can be reduced and contrast can be enhanced. Techniques that without AO are to slow for live imaging might now be usable, opening up completely new fields of research. Another advantage of AO lies in the microscopy design. Using AO methods, can help the designer to relax the aberration tolerance. This permits a significant reduction in the complexity of the optical system while maintaining diffraction limited operation.

This section will describe, using state of the art examples, how AO is implemented in both widefield and point scanning systems.

3.1 Widefield Microscopy

As mentioned above, AO techniques are being applied in widefield microscopy. In conventional microscopes, widefield illumination is provided using back light illumination or in the case of reflection or fluorescence modes, via the objective lens. The image quality depends only on the aberrations induced in the detection path and is independent of the aberrations of the illumination path. Aberration correction is therefore only necessary in the detection path and a single pass adaptive optics system will suffice [25]. Hence, the goal of AO for widefield microscopy is to restore the best possible imaging and to correct for aberrations induced both by an imperfect imaging system as well as by the imaged specimen. The latter becomes more important for thick biological samples where the light has to travel a larger distance through a medium with an inhomogeneous refractive index.

Many other highly specialized widefield microscopy techniques have been developed and for most of those, AO schemes for aberration correction and resolution optimization have been presented. Two widefield microscopy techniques will be presented in this section. First the implementation of AO in a standard transmission microscope (Section 3.1.2) using a sensorless wavefront sensing scheme is explained. **Write or mention part OF [26] and [27]!** How the theoretical background of this technique can be applied to more sophisticated microscopy schemes is then shown on the example of structured light illumination (Section 3.1.3), a specialized wide field technique.

For fluorescence microscopy, the aberration caused by an refractive index mismatch between sample, cover plate and immersion medium can be calculated theoretically and is then corrected [28] or the aberration is measured using a guide-start technique [27] as described in Section 2. Since the techniques applied in fluorescence microscopy are very similar to the ones presented for transmission microscopes, they will not be explicitly covered here. AO is also applicable in multifocal multiphoton microscopy [29, 30].

3.1.1 Direct Wavfront Sensing in a Transmission Microscope

[26]

While the scheme presented above has the advantages of only needing a deformable mirror and no extra wavefront sensor, it also requires a lot of time to quire the necessary $2N + 1$ images. It is also inflexible, since the model used for the optimization is depending on both the imaging system and the sample. Another approach is to use a direct wavefront sensing scheme, as presented by *Azucena et al.* in 2010 [27]. Until their publication, most AOM system only measured the wavefront indirectly due to the added complexity and the lack of natural point-source references such as the “guide-stars” used in astronomy and vision science. The authors overcome the latter problem by introducing a suitable fluorescent point source reference beacon as an artificial guide-star into the sample.

Fluorescent microspheres can be engineered in a large variety of colors and are often used in biology. The microspheres can be manufactured with coatings to preserve them in different conditions and to target different biological tissues, organelles, cell walls, or other biological structures [14]. There are also

various ways to introduce them into the sample such as negative pressure injection, pressure injection, matrotrophically and diffusion. *Azucena et al.* in particular inject small fluorescent microspheres into *Drosophila* embryos where they are diffraction limited when imaged by the Shack- Hartmann wavefront sensor. Hence they can be used as a point source, enabling effective wavefront sensing. After the microspheres were injected successfully, the applied wavefront sensing in correction technique is very similar to the one described used by *Aviles-Espinosa et al.* [31] and described in Section 3.2.2. We will therefore not further elaborate on this technique here. The final data analysis of *Azucena et al.* demonstrated that their approach can improve the Strehl ratio by 2 times on average and as high as 10 times when imaging through 100 μm of tissue.

3.1.2 Indirect Wavfront Sensing in a Transmission Microscope

To implement adaptive optics with standard (incoherent) transmission microscopes, *Debarre et al.* [14] implement an indirect, sensorless and image-based adaptive optics scheme, as shown in Fig. 7. As described earlier in Section 2.2, image-based techniques do not require an additional wavefront sensor but retrieve the correction data directly from the recorded images. As with all indirect sensing schemes, the difficulty is to find a good metric for image quality, which allows to determine the appropriate correction parameters.

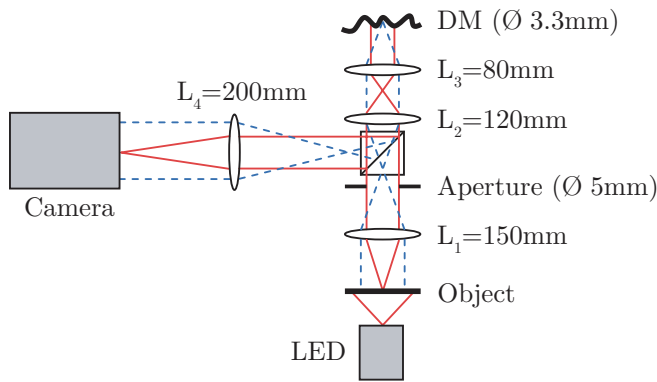


Figure 7: Schematic diagram of the experimental setup, showing a simple microscope complemented with a deformable mirror for aberration correction. Image after [14].

The presented method uses low spatial frequency content of the image as the optimization metric. The aberration is represented in terms of so called Lukosz modes. Like Zernike polynomials, the Lukosz functions are each expressed as the product of a radial polynomial and an azimuthal function. The presented technique is based on modeling the effects of aberrations on the imaging of low spatial frequencies, which Lukosz modes are found to be ideal for.

By modeling the aberration $\Phi(r)$ as a series of N Lukosz modes $L_i(r, \phi)$ with coefficients a_i [22]:

$$\Phi(r) = \sum_{i=4}^{N+3} a_i L_i(r, \phi), \quad (3.1)$$

they develop the optimization metric g as the sum of a range of low frequencies. It is related to the coefficients of the aberration expansion, a_i by the Lorentzian function [14]

$$g(a_i) \approx \frac{1}{q_0 + q_1 \sum_{i=4}^{N+3} a_i^2} \quad (3.2)$$

where the piston, tip and tilt modes ($i = 1, 2, 3$ respectively) have been omitted and q_0 and q_1 are both positive quantities in the frequency range of interest. The aberration correction process is then performed as the maximization of $g(a_i)$. Because of this particular aberration expansion and optimization metric, the function $g(a_i)$ shows a paraboloidal maximum that permits the use of simple maximization algorithms. Furthermore, it is shown that the optimization can be performed as a sequence of

independent maximizations for each aberration coefficient.

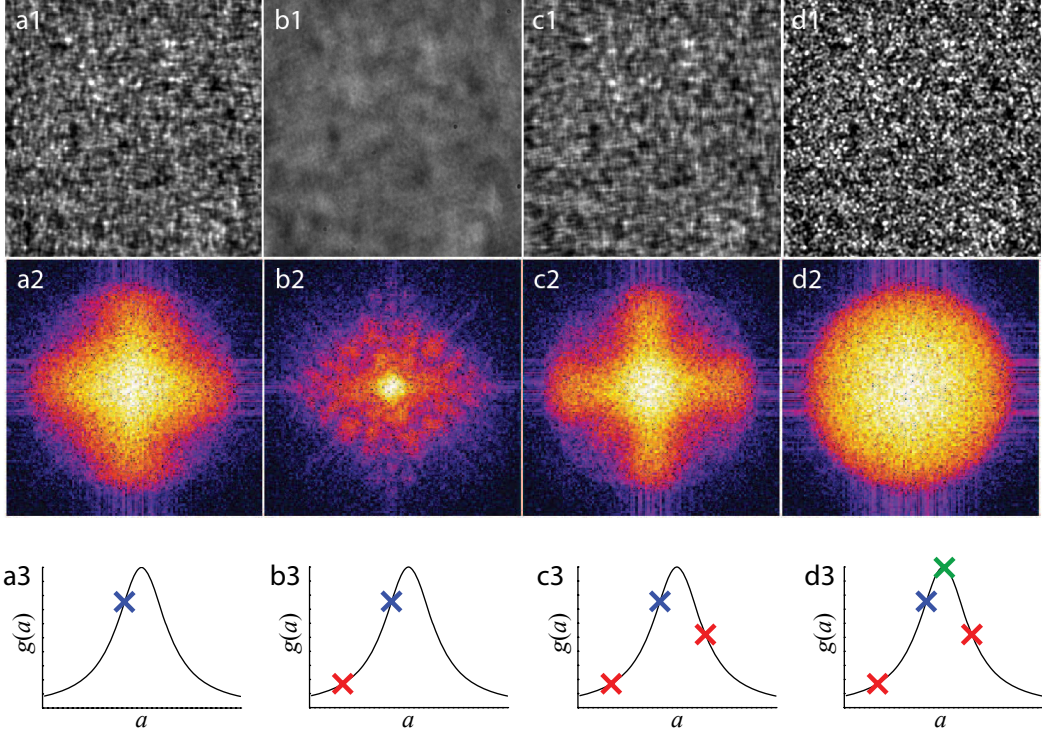


Figure 8: Correction of a single Lukosz aberration mode (astigmatism, $i = 5$) for a scatterer specimen and using low spatial frequencies. The first row shows the raw images of the specimen and the second row contains the corresponding spectral densities. The third row illustrates schematically the sampling of the Lorentzian curve used in the optimization calculation. (a1-a3) correspond to an arbitrary initial aberration of magnitude, (b1-b3) have an additional negative bias while (c1-c3) have an additional positive bias of equal magnitude. (d1-d3) show the corrected image calculated with the parabolic minimization. Image after [14].

The correction process is shown in Figure 8 for the correction of a single Lukosz mode using a scatterer specimen. Using the deformable mirror (DM), an initial aberration a_i is applied and an image is recorded. The Fourier transform and spectral density of the image are then calculated and the appropriate range of frequency components are summed, giving the metric measurements g_0 . The same procedure is repeated with both negative and positive aberrations (i.e. stronger and weaker aberrations), resulting in the metric measurements g_- and g_+ . Due to the parabolic maximum of Eq. (3.2), the value of a_i that minimizes g can be calculated from as little as three measurements of $g(a_i)$. The optimum correction aberration can then be estimated by parabolic minimization as [23]:

$$a_{\text{corr}} = \frac{b(g_+ - g_-)}{2g_+ - 4g_0 + 2g_-} \quad (3.3)$$

and is then applied to the DM. To correct multiple modes, each modal coefficient is measured in the same manner before the full correction aberration containing all modes is applied. While this technique is based only on low spatial frequencies, it is shown that both low and high frequency components can be effectively corrected. In all the cases investigated, a Strehl ratio greater than 0.8, close to the diffraction limit, was obtained. This indicates that, when aberration statistics are unknown, choosing small spatial frequencies for an initial correction is a reasonable strategy. If further correction is required, they can be performed using a larger range of frequencies. *Debarre et al.* conclude that this correction scheme is largely independent of the object structure and propose that this approach also to be valid for coherent or partially coherent systems.

3.1.3 Structured Illumination Microscopy

It is often desired for biological samples to produce clear images of focal planes deep within a thick sample (i.e. optical sectioning) and common techniques include point-scanning techniques such as confocal or multiphoton techniques which are described in Section 3.2.

Widefield techniques such as Structured Illumination (SI) microscopy can also provide optical sectioning. However, there the sectioning is realized using a standard microscopes, an incoherent light source and without the need for a scanning mechanism. For SI microscopy, a grid is imaged into the specimen to produce a one-dimensional sinusoidal excitation pattern in the focal plane. The resulting sinusoidal fluorescence image, consisting of both in-focus and out-of-focus fluorescence emission, is then normally recorded. Several images are taken, each corresponding to a different grid position equivalent to three different phase shifts of the grating. The grid pattern only appears in the focal plane while it is blurred in the out of focus regions. Hence, it is possible to extract an optical section from the spatially modulated component of the images via a simple calculation.

Based on the SI microscopy technique presented by *Neil et al.* in 2005 [32] as well as their earlier work on indirect wavefront sensing using a conventional microscope [14] in 2007 (described in the previous section) *Debarre et al.* combined both techniques in 2008 and proposed an AO scheme for use in SI microscopy [33].

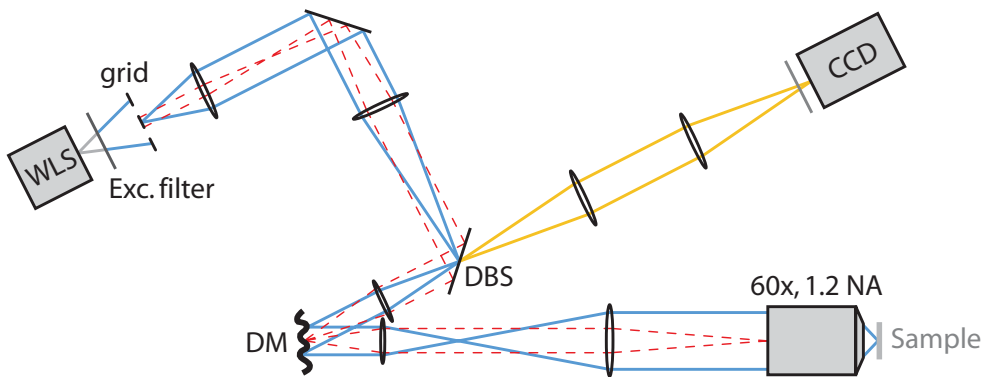


Figure 9: Experimental setup for structured illumination microscopy with aberration correction. WLS - white light source, DM - deformable mirror, DBS - dichroic beamsplitter. The blue rays mark the illumination path; the detection path is shown in yellow. Image after [33].

They again present a sensorless wavefront detection scheme, which is shown in Fig. 9. The method to obtain the aberration correction is similar to the one presented and explained in the previous section. The authors derive an inner product from a mathematical model of the imaging process, followed by an orthogonalization process applied to a set of Zernike polynomials. Based on that, a general method providing an optimal aberration expansion for the chosen optimization metric is presented. This process yields information about the effects of different aberration modes in of the SI microscope. *Debarre et al.* show that the image quality mainly depends on the imaging efficiency spatial frequency of the illumination pattern. This imaging efficiency is affected much more by some aberration modes (called grid modes) than by others (called non-grid modes). Grid modes have a significant influence on the intensity of the sectioned image, whereas non-grid modes have comparatively little effect. The non-grid modes do however affect the resolution.

The results of the implemented AO scheme is shown in Fig. 10 for aberration correction on a fluorescent mouse intestine. The image contrast and sharpness improvement is clearly visible in image 10b compared to the uncorrected image in 10a. As a result of the aberration correction, and as shown in Fig. 10c, the contrast of small sample features (blue arrows) is better defined after (red solid line) rather than before (black dotted line) correction.

The authors also explain an additional benefit of aberration correction for structured illumination microscopy. That the adaptive element can also be used to improve the rejection of the out-of-focus fluorescence. When imaging thick specimen, noise fluctuations in the fluorescence signal between the three successive widefield images obtained for the maximization process result in a large out-of-focus

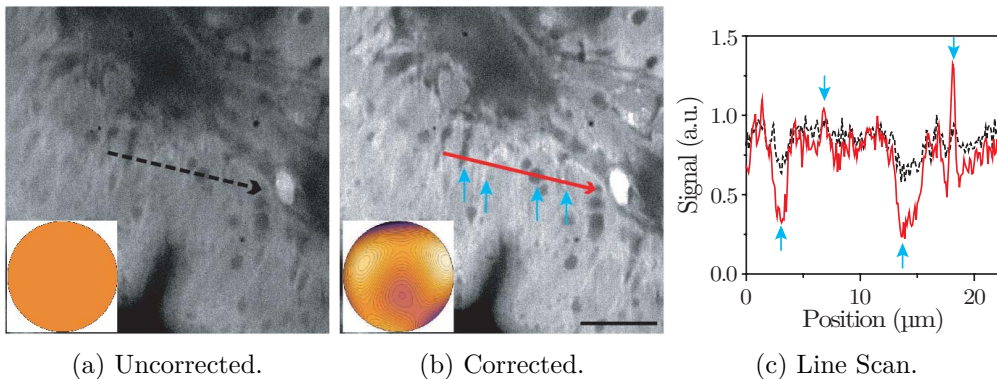


Figure 10: Aberration correction in structured illumination microscopy. A fluorescent mouse intestine sample was imaged (a) without (b) with aberration correction with inserts showing the phase induced by the deformable mirror. (c) Profile along the lines drawn on the images, both profiles normalized so that their mean value is identical. As a result of the resolution improvement, the contrast of small sample features (blue arrows) is better defined after (red solid line) rather than before (black dotted line) correction. The imaging depth was approximately 10 μm , scale bar size 10 μm . Image after [33].

background in the calculated sectioned images. Since this background arises from fluorescence generated outside the focal plane, it is not sensitive to the presence of aberrations. By applying large aberrations in a number of grid modes, the grid pattern is suppressed and only the out-of-focus noise can be measured. By subtracting this aberrated image from the original sectioned image, the fluorescent background can be efficiently removed, leading to greatly improved contrast of the in-focus structures.

The aberrations can also change significantly with depth and hence using the same correction for different depths can result in a degradation of the image quality. The correction can however be adapted for different imaging depths in the sample. This permits improvement of the image quality throughout an axially extended sample. It is furthermore possible to determine the appropriate modes once and use the same scheme for any specimen, as the scheme is mostly independent of the object structure. Alternatively, if one wants to correct for local variations in aberrations the image could be formed from several sub-images for which independent aberration correction would be performed.

In conclusion, the authors present a sophisticated, easy to implement and highly versatile AOM scheme which allows for aberration correction induced by the optical system, the specimen or the focus depth. While the presented scheme uses a widefield microscope, *Debarre et al.* are also optimistic that similar AO methods based on indirect, image based aberration detection can be applied to point-scanning methods.

3.2 Point Scanning Microscopes

Just as with the widefield techniques, adaptive optics quickly found its way into point scanning techniques to improve the image and signal quality. Scanning methods are useful for imaging biological specimens, since they can provide high resolution imaging in three-dimensions. Illumination is usually provided by a laser that is focused into the sample. The light emitted or reflected from the specimen is collected, usually through the same objective lens, and its intensity is measured by a detector. Since this only provides information about the intensity at a single spot, the focal point is then scanned through the specimen and point-by-point the image is acquired.

This section will give a brief description how AO is applied to HG, CARS and STED microscopy. Following this will be a more detailed analysis of how adaptive optics is implemented into confocal (section 3.2.1) and two-photon fluorescence microscopes (section 3.2.2).

Adaptive optics techniques have been developed for all common point scanning microscopes. Using both the second- and third-harmonic intensity signals as the optimization metric for an indirect wavefront sensing scheme, *Jesacher et al.* [34] as well as *Olivier et al* [35] have shown AO applied

to higher harmonic generation microscopy. The aberration correction is compensating both system- and specimen-induced aberrations when imaging live mouse embryos. The authors demonstrate an improved signal level and resolution, with peak intensity increased by almost *unit*[50] % and the FWHM decreased by 14 % to $1.22 \mu\text{m}$ compared with a value of $1.15 \mu\text{m}$ for an unaberrated system.

Even better results were reported by *Wright et al.* [36] when applying AO to CARS. The authors achieved a signal improvement by a factor of 3 for samples at a depth of $700 \mu\text{m}$ and a factor of 6 for muscle tissue at a depth of $260 \mu\text{m}$. Their completely random optimization typically converged after 3000 changes mirror shapes. With a mirror speed of up to 1kHz this is sufficiently fast. The approach is well suited to CARS microscopy where photobleaching does not occur but is less applicable for other microscopy techniques.

It is also possible to apply AO to STimulated Emission Depletion (STED) microscopy (see [37] for basic working principle of STED) as recently presented by *Gould et al.* [38], again employing an indirect sensing scheme. Using a phase mask, the authors both created the doughnut shape depletion beam and simultaneously realize an aberration correction. Using an additional spatial light modulator, aberration correction is also implemented in the excitation beam. The correction in the depletion beam leads to a better resolution while the correction of the excitation beam path results in a stronger signal and less noise. Unlike in many other indirect sensing methods, here the image brightness proved to be a poor quality metric due to the depletion. Hence the authors introduced a new metric that seeks to optimize both image brightness and image sharpness in a combined approach. The new approach worked successfully resulting in a $\tilde{5}$ -fold increase in the peak signal as well as a $\tilde{3.2}$ -fold improvement in resolution.

3.2.1 Confocal Microscopes

The first attempt to apply AO in confocal microscopy was done by *Martin J. Booth et al.* [39]. They implemented indirect wavefront sensing to a confocal fluorescence microscope in a closed-loop way. Aberration measurement and correction was done sequentially. First a preset positive bias aberration was introduced by a deformable membrane mirror. An image was taken and all of its pixel values were summed and averaged to give the value of W_1 . Then, it was added to the system the equivalent negative bias aberration, obtaining W_2 . They had shown before that the value of the difference signal, $W = W_1 - W_2$, is approximately proportional to the amount of the Zernike mode Z_i present in the sample. They applied this procedure for several different Zernike modes, updating the mirror shape each time. A simple representation of the experimental set-up is shown in Fig. 11.

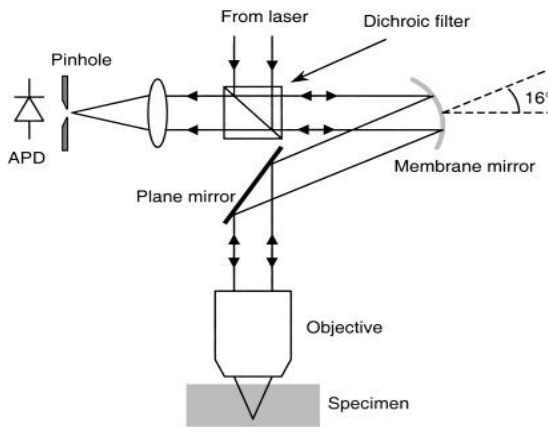


Figure 11: The illumination beam was passed through a beam expander and reflected by the membrane mirror such that the angle between the incident and reflected beams was 16° . Then it passed into the objective lens focusing the light into the specimen. Fluorescence light from the specimen was collected by the same objective. In this configuration, the membrane mirror can compensate for aberrations introduced into both the illumination and emission optical paths.

With this sequential method for correcting aberrations they achieve a 1.8 times smaller axial PSF, using two cycles of this modal wavefront sensor applied to low order aberration modes.

A different way to apply AO in confocal microscopy was done by *Xiaodong Tao et al* [40]. They used a direct wavefront sensor in a fluorescence confocal microscope. Particularly, they implemented a Shack-Hartmann sensor with fluorescent micro-spheres ($1\text{ }\mu\text{m}$ diameter) embedded in the sample as a point source reference beacons. Their set-up was designed to operate in a close-loop. The corrector device was a deformable mirror. A separate laser channel was added to excite the microsphere, which shared the same light path with the imaging channel. The results showed a 4.3 x improvement in the Strehl ratio and a 240 % improvement in the signal intensity for fixed mouse tissues at depths of up to $100\text{ }\mu\text{m}$. Although the effects of these microspheres in the live tissue have to be further investigated, this direct method enabled a shorter exposure time during sensing and a higher speed of imaging, which showed its potential ability for live in vivo imaging.

The confocal microscopy can be operated in reflection or fluorescence mode. Both are a dual pass system, which means that either the illumination path and the emission path have to be corrected in an AO confocal microscope.

3.2.2 Two-Photon Fluorescence Microscopy

Its intrinsic optical sectioning, larger penetration depth, reduced photo damage as well as other advantages allowed nonlinear microscopy in general, and Two-Photon Fluorescence Microscopy (TPFM) in particular, to become a very important tool in biological imaging since its first presentation by *Denk et al.* in 1990 [41]. As with most AO microscopy techniques, both a direct and indirect wavefront sensing scheme can be deployed for the use with TPFM. Indirect sensing was already explained (section 2.2) and presented (section 3.1 in detail). *Marsh et al.* present the first and fairly simple indirect sensing approach, correcting only for depth induced aberrations as early as 2003 [42]. Again, based on their earlier works ([14, 33]), *Débarre et al.* present another highly sophisticated application of their image based wavefront sensing scheme in 2009 [43]. Since both *Marsh* and *Débarre* essentially use the standard TPFM setup and the image optimization is very similar to the one presented earlier, we will not describe these methods here again. *Rueckel et al.* present a wavefront correction method using coherence-gated wavefront sensing [13] which also beyond the scope of this report. This section will therefore describe direct wavefront sensing based on the work presented by *Aviles-Espinosa et al.* in 2011 [31].

For two-photon fluorescence microscopy, it is not essential to correct for sample or system induced aberrations on the collected beam. Since it is a point scanning technique, all the light emitted in the focus region is collected and only the relative intensity difference is important for the generation of the image (see [44] for a detailed review on TPFM). To achieve the highest possible resolution, especially when imaging deep in a tissue, it is however very important to correct aberrations of the excitation beam. This will not only result in a better, i.e. smaller focus spot, but will also highly increase the efficiency of the nonlinear process. As described in earlier sections, a indirect wavefront sensing is usually applied for microscopic applications, and such a system developed by *Sherman et al.* [45] will be presented in the next section. To overcome some of the inherent disadvantages of indirect sensing, *Aviles-Espinosa et al.* developed a direct sensing scheme for two-photon fluorescence microscopy as described in section

3.2.3 Multiphoton Scanning Microscopy using Indirekt sensing.

[45, 46]

[46] since it is also given as reference in [45].

[45] We demonstrate adaptive aberration correction for depthinduced spherical aberration in a multiphoton scanning microscope with a micromachined deformable mirror. Correction was made using a genetic learning algorithm with two-photon fluorescence intensity feedback to determine the desired

shape for an adaptive mirror. For a 40x, 0.6 NA long working distance objective, the axial scanning range was increased from 150 mm to 600 mm.

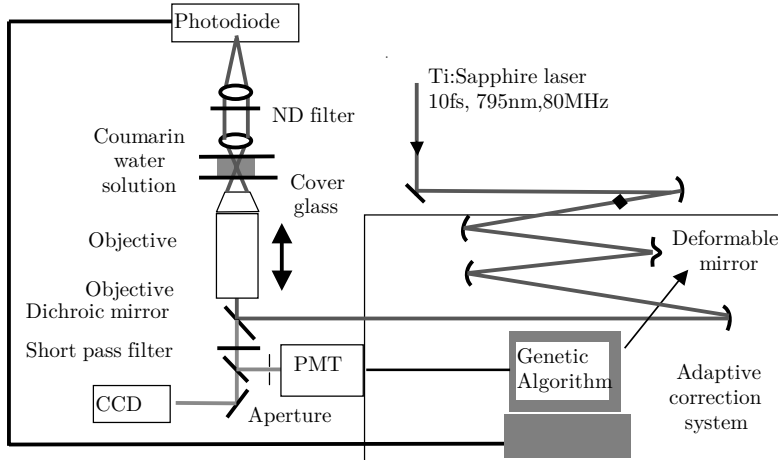


Figure 12: The experimental system consisting of the 10 fs oscillator with dispersion compensation, the adaptive correction system including the deformable mirror, and the confocal microscope with long working distance 40x air immersion objective. Image after [45].

In this paper we show a technique for dynamic specimen induced spherical aberration correction without the use of a wavefront measurement and the subsequent loss of power. A deformable mirror is used for the dynamic wavefront correction with a genetic algorithm (GA) that maximizes the two-photon signal from the sample to determine the appropriate wavefront. This method was first used for adaptive correction of off-axis aberrations[46]. Together, the dynamic correction for depth-induced spherical aberration and off-axis aberrations can provide for full adaptive aberration compensation over a 3D volume.

The microscope system in this work uses a dry 40 x /0.6 NA infinity corrected Olympus long working distance objective designed to look deep into samples such as tissues. For simplicity we use a Coumarin water solution in place of the biological sample that is commonly analysed with multiphoton fluorescence microscopy. The long working distance objective allows one to scan from the surface of the cover glass up to 2 mm into the sample. Two-photon fluorescence is collected with the objective, passes through a dichroic mirror and a short pass filter, is imaged through a confocal aperture to reduce out-of-focus background and measured with a photomultiplier tube (PMT), or is imaged onto a CCD camera. A photodiode is used to monitor the transmitted fundamental light through the sample for normalization of the two-photon fluorescence.

We use all reflective optics, except in the objective, to limit pulse broadening due to dispersion. This adds a small amount of astigmatism to the beam. This astigmatism and other small aberrations due to misalignment can be corrected with the DM in the form of a static correction, made when the focus is close to the surface of the sample and no depth-induced spherical aberration is present.

Instead of the traditional approach in adaptive optics of measuring the wavefront and calculating the correction needed, we use a genetic algorithm (GA) with two-photon fluorescence as feedback to determine the optimum shape for the mirror to compensate for any aberrations in the system. This eliminates the need for a formal wavefront measurement because the two-photon signal will increase due to tighter focusing.

Dynamic aberration is achieved by running the GA to determine the DM wavefront that would best maximize the twophoton intensity at the focus as measured by the fluorescence power. The GA is an evolutionary learning algorithm that starts with a set of random solutions for the DM wavefront as first ‘parents’. The random solution is revised by mating the solutions together to obtain a larger set of ‘offspring’. These offspring are then tested on the system and the ones that produce the largest two-photon fluorescence intensity at focus are saved to provide the parents for the next generation of offspring. This continues until the two-photon intensity reaches a steady maximum value. This is reiterated for steps of deeper focusing within the specimen. An optimum DM solution will emerge in

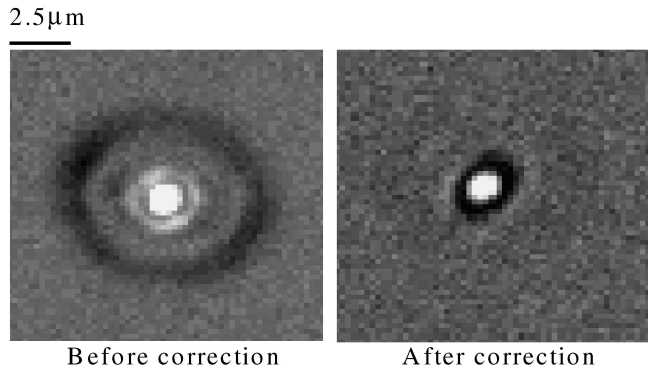


Figure 13: Normalized CCD image of two-photon fluorescence at a focus depth of 600 mm with and without correction with the DM. [45]

approximately 10 generations (approximately 3 min, and can be saved for future use, as long as the objective is the same and the location of the DM in relation to the microscope has not been changed. (Further details of the GA implementation may be found in Albert et al. , 2000).

We next confirmed that the use of the DM to maximize the two-photon fluorescence does indeed increase the imaging resolution. The improved resolution in a CCD image of the two-photon fluorescence at 600 μm is shown in Fig. 13

longitudinal PSF was measured with third harmonic generation (THG). THG occurs only at an interface with index of refraction difference at the focus of the laser. For this measurement a quartz plate was scanned from one side of the focus to the other. The normalized longitudinal PSFs clearly indicate an increase of resolution with correction. An example, Fig. 9, shows (at a focus depth of 350 mm) near-diffraction-limited FWHM of the longitudinal PSF of 6.5 mm achieved with dynamic aberration correction, whereas the FWHM is 12.7 mm for the uncorrected case.

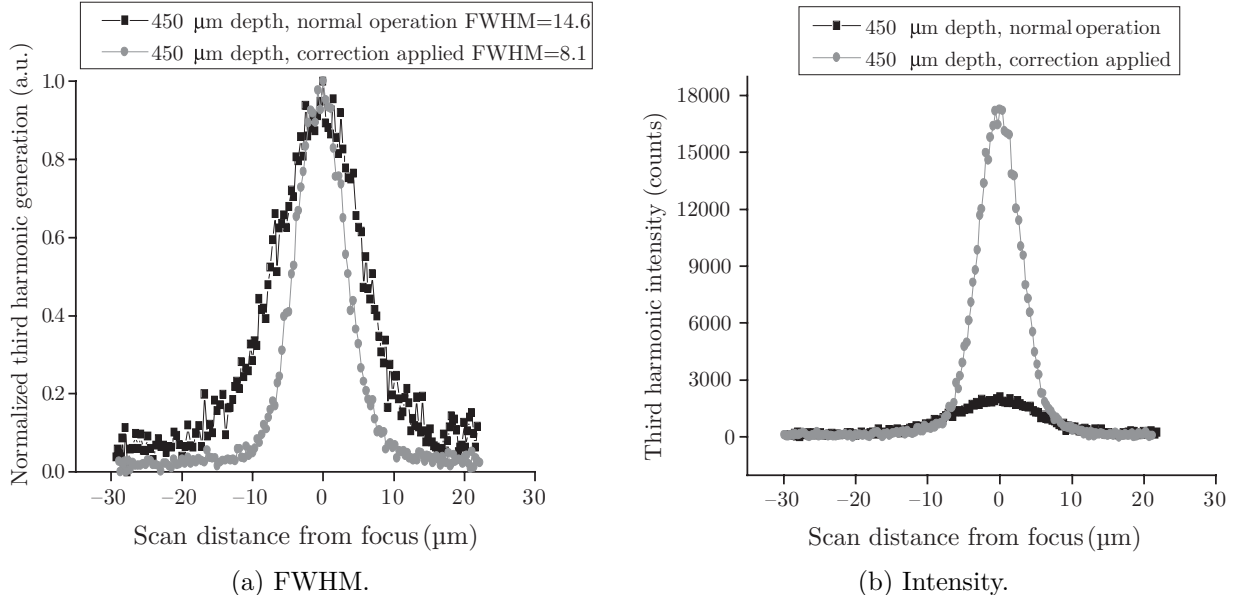


Figure 14: Normalized longitudinal point spread for focusing depth of 450 mm for both corrected and uncorrected showing increase in resolution due to correction, as well as unnormalized showing increase in intensity due to correction [45].

3.2.4 TPFM Direct

While indirect sensing has several advantages over direct sensing (see sec. 2.2), they have one important drawback that can ultimately not be overcome. They all depend on an iterative optimization procedure

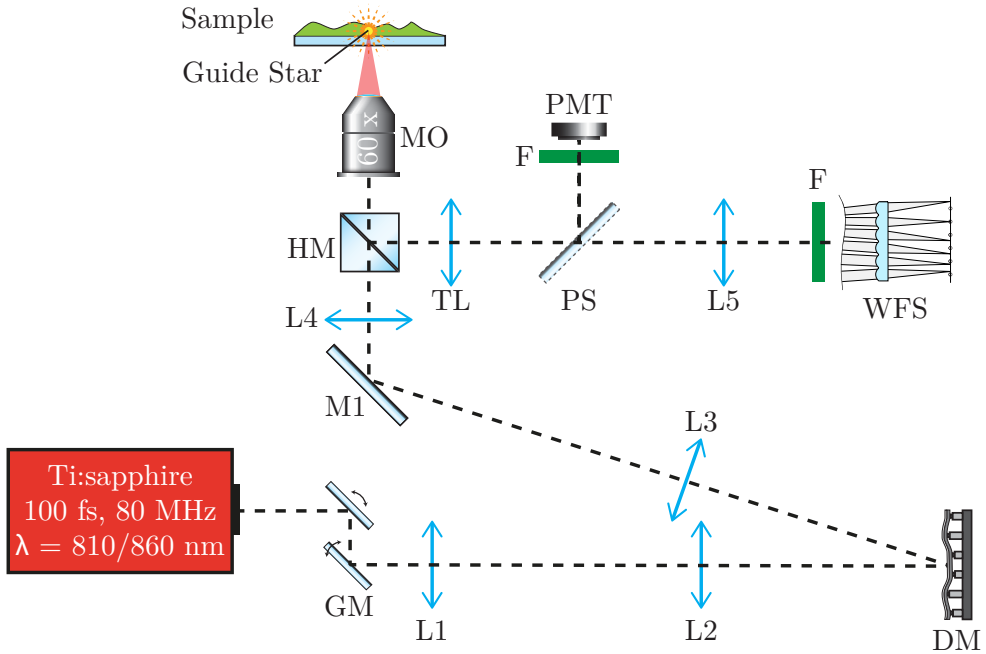


Figure 15: Experimental setup for aberration corrected two-photon fluorescence microscopy as proposed by *Aviles-Espinosa et al.*. GM - galvanometric mirrors, L1-L5 - lenses, DM - deformable mirror, M1 - mirror, HM - filter and beamsplitter, MO - microscope objective, TL - microscope tube lens, F - band pass filters, PMT - photo multiplier tube, WFS - Shack-Hartmann wavefront sensor. The microscope output port is manually selected either for the PMT or for the WF sensor using PS. See [31] for the original image as well as a detailed description of the working principle.

to estimate and correct for the aberrations. While random optimization requires many iterations (in some cases up to 3000 iterations per mirror actuator [36]) other methods base the iterations on complicated models and are able to achieve indirect sensing with as little as $2N + 1$ iterations (where N is the number of corrected aberration modes) [14, 33, 43]. However, even these methods require the sample to be exposed and imaged multiple times. To correct 11 aberration modes (as done in [43]), one needs 23 exposure to acquire an aberration corrected image. While this is suitable for some systems such as CARS where photobleaching is not an issue, it often limits the feasibility of AO in fluorescence imaging. Being aware of these limitations, *Aviles-Espinosa et al.* therefore developed a direct sensing scheme.

As described in section 2.1, to be able to use a wavefront sensor, one needs a point like reference source which is then used to detect the aberration. This point like source, called “nonlinear guide star” “(NL-GS) by the authors¹, can be artificially created and imbedded in the sample, as done for standard fluorescence microscopy [27]. This however can cause damage to the sample or might influence the behavior of living samples, limiting its potential for *in vivo* imaging. *Aviles-Espinosa et al.* realized that two-photon excited fluorescence naturally produces a small confined volume which can be used as the guide-star. The setup presented by the authors is shown in Fig. 15. The setup shown is basically an inverted microscope, modified to be used as laser scanning TPFM (see paper for detailed component description and working principle). A mode locked Ti:sapphire laser ($\lambda = 810$ nm & 860 nm, pulse duration = 100 fs, repetition rate = 80 MHz, average powers in sample plane = 1.5 mW to 5.6 mW) is used as the excitation beam. The wavefront sensing is performed using a Shack-Hartmann WaveFront Sensor (SH WFS), located at one of the output ports of the microscope. The aberration correction is realized with an electromagnetic Deformable Mirror (DM).

Before the authors started their experiments on biological samples, they first showed that the guide star is reproducible, reliable and independent from the excitation beam aberrations. They continued

¹The term “guide start” is used in reference to astronomy. There a star or a laser spot projected in the sky is used as the reference and called guide star.

to verify that the NL-GS behaves as point source as well as proving that aberrations are similar in the complete Field Of View (FOV). Since all these requirements were met, it was shown that aberrations in the imaged area can be effectively corrected using only one NL-GS. The authors then continued to calibrate their system, eliminating the passive aberrations of the microscope system coming from the optics for excitation beam as well as the beam path from the objective pupil to the output ports of the microscope. These so called coupling aberrations only need to be corrected once for a given microscopic setup. They were measured and taken into account as a reference for all the subsequent wavefront measurements. The second correction step was to measure the so called focusing aberrations caused by the focusing part of the system. This step was performed every time prior to the actual image acquisition to account for the specific measurement (i.e. the objective, the refractive index matching oil, the cover slip and the sample).

The authors then investigated the performance of their AOM system using both *Caenorhabditis elegans* and mouse brain samples. -For small aberrations and weak scattering only a modest improvement in signal intensity was shown. At an imaging depth of 25 μm , the measured signal enhancement was 1.75x by correcting the coupling aberrations, and 3.61x when focusing aberrations were corrected as well. Similar values were obtained imaging deeper into the tissue.

Caenorhabditis elegans tissue scatterers only weakly and hence spherical aberration is the main aberration for imaging deep into the tissue. Since these should be easily corrected using the presented scheme, the authors were surprised by these relatively small improvements in the signal quality. By using an additional agar pad to simulate moderate scattering as well as imaging deeper into the tissue, the authors investigated the correction efficiency further. Deep in the sample (127 μm) where large sample induced aberrations are prominent, improvements of the signal intensity by a factor of 22.59 were possible, as shown in Fig. 16. It is noteworthy, that the aberration correction increases the signals local maxima while the local minima remain unaltered.

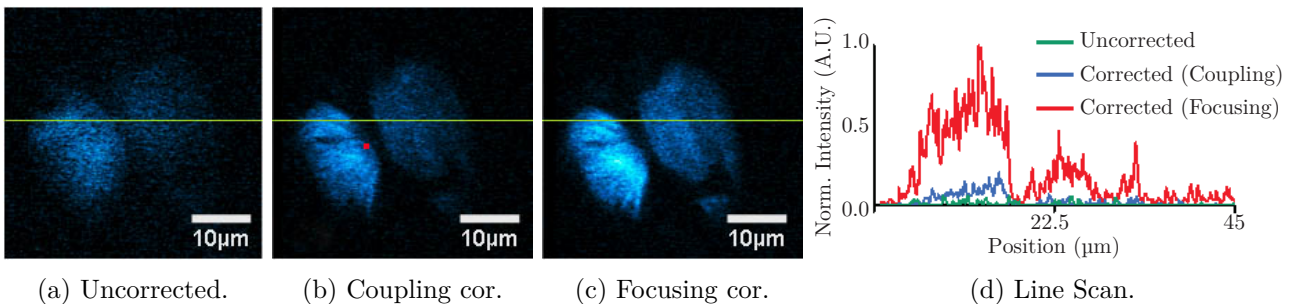


Figure 16: *In vivo* *C. elegans* sample imaged at 127 μm depth. (a) shows the uncorrected image of a worm section, (b) displays the same section with coupling correction applied and (c) shows the section when both coupling and focusing aberrations are corrected. (d) shows the intensity profile along the green line in the images for all three correction cases. The correction of coupling aberrations improves the signal intensity by a factor of only 1.94 whereas the correction of both coupling and focusing aberrations results in a very good improvement of 22.59. Image after [31].

Finally, the authors investigate the AO system performance using strongly scattering mouse brain tissue. They show that a correction is still possible, but it is less efficient than for moderately scattering samples. It is furthermore possible to record aberration corrected images with a single exposure, no need for complex optimization algorithms and without further sample preparation (i.e. no fluorescent beads need to be inserted). This minimize photobleaching effects, photo-toxicity and limits negative effects to the living sample. Since no model is needed to correct the aberrations, the method is robust and can be applied to fixed and *in vivo* biological samples. An overall intensity improvement of more than one order of magnitude was shown in some cases. In conclusion, the authors present and flexible and versatile application of adaptive optics in microscopy which can be used in wide range biological imaging applications where a high resolution is required.

4 Conclusion & Future Prospects

While adaptive optics has been applied in many fields for more than fifteen years, in biological imaging it is still a relatively new system. Since new AO techniques for modern microscopes are just being developed, it will take more time before AO can become a standard component of laboratory microscopes.

It is important to remark that AO applied to microscopy does not overcome the diffraction limit but rather helps to restore a diffraction limited imaging case. It therefore usually yields in an improvement in both axial and lateral resolution as well as an increase in signal intensity. In other words, AO extends the capabilities of high-resolution or superresolution techniques, especially extending the ability to image deeper into tissue. The advantages of correcting aberrations always depend on the specimen under study and the microscopy technique used. One of the most critical issues in AO applied to microscopy is the accuracy in the sensing process, that is, how we obtain the aberration information from the sample. It seems to be that indirect sensing is the first option in almost all the experiments for AO microscopes. This is because it is easier to implement in microscopy since it only requires a deformable mirror. Indirect sensing is however usually slower than direct sensing.

An important drawback in most AO methods for microscopy is the relatively slow wavefront detection. As long as aberrations don't change quickly or when just considering a small region of a sample, this is not a problem. However, when imaging larger parts of a sample or when trying to image fast processes in live samples, AO techniques are often too slow. Thus, it is important to further optimize current system or to develop completely new, faster correction and sensing devices (using multiple correctors being a possible solution). This would extend the ability to correct aberrations in real time and with less exposure of the specimens during the measurement. Furthermore, AO methods have not been implemented in techniques such as STORM and PALM yet. First publications in these fields are only a matter of time and are probably due to the young age of the methods, as AO techniques are currently being developed [47].

It is difficult to give specific advice regarding the choice of the correct adaptive optics system. If measurement speed and photobleaching are a concern, direct sensing should be considered, with the possible downside of a higher complexity and the need for a guide star. If a maximal signal intensity is more important and photobleaching is not a problem and if space, hardware and budget are limited, indirect sensing might be the better choice. It offers a cheap and easy AO implementation if time is not a concern or if suitable optimization algorithms can be developed. In the end, the right choice has to be determined based on the microscopy technique and system constraints. Despite all this, further improvements in the sensing and correction process will certainly further extend the already wide range AO applications in modern microscopes in the future.

References

- [1] M. J. Booth. *Adaptive Optics in Microscopy*, pp. 295–322. Wiley-VCH Verlag GmbH & Co. KGaA. ISBN 9783527635245 (2011). URL <http://dx.doi.org/10.1002/9783527635245.ch14>.
- [2] H. W. Babcock. “The possibility of compensating astronomical seeing.” *Pub. Astron. Soc. Pacific* (Oct 1953). vol. 65. URL <http://dx.doi.org/10.1086/126606>.
- [3] L. N. Thibos. “Principles of hartmann-shack aberrometry.” *Vision Science and its Applications* (2000). URL <http://www.opticsinfobase.org/abstract.cfm?URI=VSIA-2000-NW6>.
- [4] B. C. Platt & R. Shack. “History and principles of shack-hartmann wavefront sensing.” *Journal of refractive surgery* (Oct. 2001). vol. 17(5). URL <http://view.ncbi.nlm.nih.gov/pubmed/11583233>.
- [5] F. Roddier. “Curvature sensing and compensation: a new concept in adaptive optics.” *Appl. Opt.* (Apr 1988). vol. 27(7):pp. 1223–1225. URL <http://dx.doi.org/10.1364/AO.27.001223>.
- [6] I. Weingaertner & M. Schulz. “Interferometric methods for the measurement of wavefront aberrations.” *Proc. SPIE* (1993). vol. 1781:pp. 266–279. URL <http://dx.doi.org/10.1117/12.140978>.
- [7] M. J. Booth. “Wavefront sensorless adaptive optics for large aberrations.” *Opt. Lett.* (Jan 2007). vol. 32(1):pp. 5–7. URL <http://dx.doi.org/10.1364/OL.32.000005>.
- [8] M. J. Booth, D. Débarre et al. “Adaptive optics for biomedical microscopy.” *Opt. Photon. News* (1 2012). vol. 23(1):pp. 22–29. URL <http://dx.doi.org/10.1364/OPN.23.1.000022>.
- [9] F. Zernike. “Beugungstheorie des schneidenverfahrens und seiner verbesserten form, der phasenkontrastmethode.” *Physica* (1934). vol. 1(7–12):pp. 689 – 704. URL [http://dx.doi.org/10.1016/S0031-8914\(34\)80259-5](http://dx.doi.org/10.1016/S0031-8914(34)80259-5).
- [10] R. Tyson. *Adaptive Optics Engineering Handbook (Optical Science and Engineering)*. CRC Press, 1 edn. (11 1999). ISBN 9780824782757.
- [11] J. Porter, H. Queener et al. *Adaptive Optics for Vision Science: Principles, Practices, Design and Applications (Wiley Series in Microwave and Optical Engineering)*. Wiley-Interscience, 1 edn. (7 2006). ISBN 9780471679417.
- [12] D. Malacara, editor. *Optical Shop Testing (Wiley Series in Pure and Applied Optics)*. Wiley-Interscience, 3 edn. (7 2007). ISBN 9780471484042. URL <http://dx.doi.org/10.1002/9780470135976>.
- [13] M. Rueckel, J. A. Mack-Bucher et al. “Adaptive wavefront correction in two-photon microscopy using coherence-gated wavefront sensing.” *Proceedings of the National Academy of Sciences* (2006). vol. 103(46):pp. 17137–17142. URL <http://dx.doi.org/10.1073/pnas.0604791103>.
- [14] D. Debarre, M. J. Booth et al. “Image based adaptive optics through optimisation of low spatial frequencies.” *Opt. Express* (6 2007). vol. 15(13):pp. 8176–8190. URL <http://dx.doi.org/10.1364/OE.15.008176>.
- [15] J. R. Fienup & J. J. Miller. “Aberration correction by maximizing generalized sharpness metrics.” *J. Opt. Soc. Am. A* (Apr 2003). vol. 20(4):pp. 609–620. URL <http://dx.doi.org/10.1364/JOSAA.20.000609>.
- [16] D. Whitley. “A genetic algorithm tutorial.” *Statistics and Computing* (1994). vol. 4(2):pp. 65–85. URL <http://dx.doi.org/10.1007/BF00175354>.

- [17] A. J. Wright, D. Burns et al. “Exploration of the optimisation algorithms used in the implementation of adaptive optics in confocal and multiphoton microscopy.” *Microscopy Research and Technique* (2005). vol. 67(1):pp. 36–44. URL <http://dx.doi.org/10.1002/jemt.20178>.
- [18] J. Li & H. Chen. “A closed-loop adaptive optical system based on genetic algorithm.” In “Electrical and Control Engineering (ICECE), 2010 International Conference on,” (2010) pp. 16–18. URL <http://dx.doi.org/10.1109/ICECE.2010.12>.
- [19] F. Gonté, A. Courteville et al. “Optimization of single-mode fiber coupling efficiency with an adaptive membrane mirror.” *Optical Engineering* (2002). vol. 41(5):pp. 1073–1076. URL <http://dx.doi.org/10.1117/1.1466462>.
- [20] P. Villoresi, S. Bonora et al. “Optimization of high-order harmonic generation by adaptive control of a sub-10-fs pulse wave front.” *Opt. Lett.* (Jan 2004). vol. 29(2):pp. 207–209. URL <http://dx.doi.org/10.1364/OL.29.000207>.
- [21] M. Booth. “Wave front sensor-less adaptive optics: a model-based approach using sphere packings.” *Opt. Express* (Feb 2006). vol. 14(4):pp. 1339–1352. URL <http://dx.doi.org/10.1364/OE.14.001339>.
- [22] W. Lukosz. “Der einfluß der aberrationen auf die optische Übertragungsfunktion bei kleinen ortsfrequenzen.” *Optica Acta: International Journal of Optics* (1963). vol. 10(1):pp. 1–19. URL <http://dx.doi.org/10.1080/713817744>.
- [23] W. H. Press, S. A. Teukolsky et al. *Numerical Recipes 3rd Edition: The Art of Scientific Computing*. Cambridge University Press, 3 edn. (9 2007). ISBN 9780521880688. URL <http://www.nr.com/>.
- [24] M. Schwertner, M. Booth et al. “Characterizing specimen induced aberrations for high na adaptive optical microscopy.” *Opt. Express* (12 2004). vol. 12(26):pp. 6540–6552. URL <http://dx.doi.org/10.1364/OPEX.12.006540>.
- [25] V. N. Mahajan. *Optical Imaging and Aberrations, Part II. Wave Diffraction Optics (SPIE Press Monograph Vol. PM209)*. SPIE Press, 2 edn. (8 2011). ISBN 9780819486998. URL <http://dx.doi.org/10.1117/3.898443>.
- [26] O. Azucena, J. Crest et al. “Adaptive optics wide-field microscopy using direct wavefront sensing.” *Opt. Lett.* (Mar 2011). vol. 36(6):pp. 825–827. URL <http://dx.doi.org/10.1364/OL.36.000825>.
- [27] ——. “Wavefront aberration measurements and corrections through thick tissue using fluorescent microsphere reference beacons.” *Opt. Express* (Aug 2010). vol. 18(16):pp. 17521–17532. URL <http://dx.doi.org/10.1364/OE.18.017521>.
- [28] P. KNER, J. SEDAT et al. “High-resolution wide-field microscopy with adaptive optics for spherical aberration correction and motionless focusing.” *Journal of Microscopy* (2010). vol. 237(2):pp. 136–147. URL <http://dx.doi.org/10.1111/j.1365-2818.2009.03315.x>.
- [29] J. Bewersdorf, R. Pick et al. “Multifocal multiphoton microscopy.” *Opt. Lett.* (5 1998). vol. 23(9):pp. 655–657. URL <http://dx.doi.org/10.1364/OL.23.000655>.
- [30] S. Coelho, S. Poland et al. “Multifocal multiphoton microscopy with adaptive optical correction.” *Proc. SPIE* (2013). vol. 8588:pp. 858817–858817–12. URL <http://dx.doi.org/10.1117/12.2000188>.
- [31] R. Aviles-Espinosa, J. Andilla et al. “Measurement and correction of in vivo sample aberrations employing a nonlinear guide-star in two-photon excited fluorescence microscopy.” *Biomed. Opt. Express* (Nov 2011). vol. 2(11):pp. 3135–3149. URL <http://dx.doi.org/10.1364/BOE.2.003135>.

- [32] M. A. A. Neil, R. Juskaitis et al. “Method of obtaining optical sectioning by using structured light in a conventional microscope.” *Opt. Lett.* (Dec 1997). vol. 22(24):pp. 1905–1907. URL <http://dx.doi.org/10.1364/OL.22.001905>.
- [33] D. Débarre, E. J. Botcherby et al. “Adaptive optics for structured illumination microscopy.” *Opt. Express* (6 2008). vol. 16(13):pp. 9290–9305. URL <http://dx.doi.org/10.1364/OE.16.009290>.
- [34] N. Olivier, D. Débarre et al. “Dynamic aberration correction for multiharmonic microscopy.” *Opt. Lett.* (10 2009). vol. 34(20):pp. 3145–3147. URL <http://dx.doi.org/10.1364/OL.34.003145>.
- [35] A. Jesacher, A. Thayil et al. “Adaptive harmonic generation microscopy of mammalian embryos.” *Opt. Lett.* (10 2009). vol. 34(20):pp. 3154–3156. URL <http://dx.doi.org/10.1364/OL.34.003154>.
- [36] A. J. Wright, S. P. Poland et al. “Adaptive optics for enhanced signal in cars microscopy.” *Opt. Express* (12 2007). vol. 15(26):pp. 18209–18219. URL <http://dx.doi.org/10.1364/OE.15.018209>.
- [37] S. W. Hell & J. Wichmann. “Breaking the diffraction resolution limit by stimulated emission: stimulated-emission-depletion fluorescence microscopy.” *Opt. Lett.* (Jun 1994). vol. 19(11):pp. 780–782. URL <http://dx.doi.org/10.1364/OL.19.000780>.
- [38] T. J. Gould, D. Burke et al. “Adaptive optics enables 3d sted microscopy in aberrating specimens.” *Opt. Express* (9 2012). vol. 20(19):pp. 20998–21009. URL <http://dx.doi.org/10.1364/OE.20.020998>.
- [39] M. J. Booth, M. A. A. Neil et al. “Adaptive aberration correction in a confocal microscope.” *Proceedings of the National Academy of Sciences* (4 2002). vol. 99(9):pp. 5788–5792. URL <http://dx.doi.org/10.1073/pnas.082544799>.
- [40] X. Tao, B. Fernandez et al. “Adaptive optics confocal microscopy using direct wavefront sensing.” *Opt. Lett.* (Apr 2011). vol. 36(7):pp. 1062–1064. URL <http://dx.doi.org/10.1364/OL.36.001062>.
- [41] W. Denk, J. Strickler et al. “Two-photon laser scanning fluorescence microscopy.” *Science* (1990). vol. 248(4951):pp. 73–76. URL <http://dx.doi.org/10.1126/science.2321027>.
- [42] P. Marsh, D. Burns et al. “Practical implementation of adaptive optics in multiphoton microscopy.” *Opt. Express* (5 2003). vol. 11(10):pp. 1123–1130. URL <http://dx.doi.org/10.1364/OE.11.001123>.
- [43] D. Débarre, E. J. Botcherby et al. “Image-based adaptive optics for two-photon microscopy.” *Opt. Lett.* (8 2009). vol. 34(16):pp. 2495–2497. URL <http://dx.doi.org/10.1364/OL.34.002495>.
- [44] M. Oheim, D. J. Michael et al. “Principles of two-photon excitation fluorescence microscopy and other nonlinear imaging approaches.” *Advanced Drug Delivery Reviews* (2006). vol. 58(7):pp. 788 – 808. URL <http://dx.doi.org/10.1016/j.addr.2006.07.005>.
- [45] L. Sherman, J. Y. Ye et al. “Adaptive correction of depth-induced aberrations in multiphoton scanning microscopy using a deformable mirror.” *Journal of Microscopy* (2002). vol. 206(1):pp. 65–71. URL <http://dx.doi.org/10.1046/j.1365-2818.2002.01004.x>.
- [46] O. Albert, L. Sherman et al. “Smart microscope: an adaptive optics learning system for aberration correction in multiphoton confocal microscopy.” *Opt. Lett.* (Jan 2000). vol. 25(1):pp. 52–54. URL <http://dx.doi.org/10.1364/OL.25.000052>.
- [47] A. Jasaitis, G. Clouvel et al. “Extreme precision in 3d: Adaptive optics boosts super-resolution microscopy.” URL <http://bit.ly/1cQri59>. Visited on 12/11/13.